

# Optimization Based on Simulation Study of Thermal-Hydraulic Behavior in Microchannel Heat Sink

Fatima Tanveer<sup>1</sup>, Aqeel Haider<sup>2</sup>

<sup>1</sup>School of Material Science and Engineering, Northwestern Polytechnical University, Xi'an, China

<sup>2</sup>School of Civil Engineering, Northwestern Polytechnical University

\*\*\*

**Abstract** - This work presents a comprehensive numerical investigation of liquid-cooled cold plates designed for high heat-flux electronic applications. Five internal geometries, leaf-vein, rectangular, diamond, cylindrical, and triangular pin-fins, are systematically compared under identical boundary conditions to isolate geometric effects on thermal-hydraulic performance. Conjugate heat transfer simulations are performed using two substrate materials, aluminum and C1020 copper, and two coolants, PG25 and HFO-1336mzz(Z). Key metrics including temperature distribution, thermal resistance, and pressure drop are evaluated and validated through mesh independence and energy balance checks. A p-Norm-based multi-objective analysis identifies the rectangular pin-fin configuration with PG25 and C1020 as the optimal balanced design.

**Keywords:** Thermal-hydraulic performance, Pin-fin geometries, multi-objective optimization, Liquid-cooled cold plates

## 1. INTRODUCTION

The continuous miniaturization of electronic devices, coupled with rising power densities, has created increasing challenges for thermal management. As components become smaller and more powerful, the heat generated per unit rises, leading to reliability issues and reduced efficiency if heat is not effectively dissipated. Conventional approaches such as forced air cooling and liquid cooling have been widely adopted, but these methods often lack the efficiency, durability, and scalability required for next-generation applications. Localized hotspots and uneven temperature distribution remain persistent challenges in high-performance systems.

Effective thermal management has therefore emerged as a critical enabling factor for next-generation electronic systems, directly influencing efficiency, safety, and long-term stability. Traditional cooling strategies that once satisfied earlier generations of electronics are now being pushed to their operational limits, prompting an urgent need for advanced heat dissipation solutions capable of addressing localized hotspots, transient heat fluxes, and strict size and weight constraints. Within this context, the present study is motivated by the growing demand for compact, passive, and high-performance thermal

management architectures that can sustain stable operation under increasingly severe thermal conditions, thereby laying the foundation for the exploration of capillary-based and structure-optimized cooling systems as viable alternatives to conventional approaches.

Recent innovations in thermal management aim to overcome these shortcomings. For example, nanoengineered two-phase cooling systems [1] have demonstrated enhanced heat dissipation and reliability in compact electronics. Similarly, advanced cooling techniques such as liquid cold plates and thermosiphon heat sinks provide scalable solutions for high-power devices. These developments highlight the urgency of transitioning from conventional thermal management systems toward more advanced and adaptable strategies.

Building on these advancements, researchers are now focusing on structures that combine high thermal conductivity materials with optimized fluid pathways to further enhance heat spreading and reduce localized temperature peaks. Hybrid systems that integrate porous media, microchannels, pin fins or engineered capillary networks have shown the ability to stabilize temperature fluctuations even under rapidly changing heat loads. These designs improve both uniformity and transport efficiency, allowing the coolant to reach and remove heat from critical regions more effectively than traditional straight-channel or fin-based layouts. Pin-fin topologies provide more manufacturing flexibility and controllability than strict biomimetic design, enabling systematic comparison across many geometric configurations. Capillary-based cooling systems offer a promising passive thermal solution by utilizing wick-like structures and optimized flow pathways, such as biomimetic leaf-vein networks, to enhance heat transfer and mitigate hotspots formation[2]. Biomimetic cooling designs, particularly diamond-shaped pin fins, have been shown to outperform other geometries in both heat transfer and flow efficiency, offering a promising solution for high-power thermal management.[3]

Biomimetic cooling systems, particularly those using diamond-shaped pin fins, effectively balance superior heat transfer against manageable flow resistance. This geometry-based optimization is critical for enhancing thermal performance in compact electronics.[4] [5]

Integrating these optimized structures with capillary-driven flow and phase-change materials creates adaptive, high-efficiency thermal pathways. This synergistic approach significantly outperforms traditional cooling methods, offering a robust solution for next-generation thermal management under high heat loads. [6] [7] [8]

Aluminum's superior machinability enables the fabrication of intricate, porous channels that mimic biomimetic vein networks, enhancing capillary flow and thermal uniformity under high heat loads. This geometric adaptability, combined with its favorable conductivity-to-weight ratio, makes it ideal for next-generation cold plates. Future advancements will integrate these passive, optimized structures with active cooling methods to manage increasing power densities in compact electronics. [9] [10] [11].

Pin-fin geometry directly dictates the thermal-hydraulic trade-off: diamond shapes enhance heat transfer, while streamlined designs reduce flow resistance, highlighting shape optimization as a critical design lever. [12] Pin-fin geometry directly dictates the thermal-hydraulic trade-off, with square fins enhancing heat transfer and circular fins minimizing flow resistance. Optimal performance depends on scale and flow conditions, where micrometer fins excel at low Reynolds numbers and millimeter fins perform better under high flow rates. Hybrid pin-fin arrangements offer a promising pathway to balance these competing objectives for advanced electronic cooling. [13], [14], [15]

Pin-fin spacing and arrangement critically affect thermal-hydraulic performance, where staggered layouts enhance heat transfer but increase pressure drop. Optimal geometry and advanced coolants like nanofluids can significantly improve overall system efficiency. [16], [17], [18] Microchannel heat sinks are vital for dissipating high heat fluxes in modern electronics. Their performance is influenced by channel geometry, coolant selection, and the use of nanofluids. This study specifically examines how pin-fin arrangement and volume fraction affect heat transfer and pressure drop, with staggered layouts enhancing cooling at the cost of increased flow resistance. [19] [20] Quantitative evaluation of fin shapes shows that drop-shaped pins achieve the best thermal performance with the lowest thermal resistance, while circular fins provide efficient heat transfer pathways. These findings underscore that geometric optimization is critical for balancing thermal efficacy and hydraulic efficiency in advanced thermal management systems. [21] [22]

Micro heat sinks achieve optimal performance through geometry-specific design, where I-shaped pin fins enhance heat transfer while minimizing pressure drop by optimizing dimensions and orientation. Validation through numerical and experimental methods confirms the governing equations and provides reliable local and average performance data across varying operating conditions. [23] [24] [25] Employing a 3D conjugate heat

transfer model that was verified by experiments, the laminar flow and conjugate heat transfer effect on microchannel heat sinks was investigated. The exact temperature distribution, heat transport patterns, and cooling efficiency are shown by the results. [26] Rectangular, trapezoidal, and triangular microchannels are investigated numerically in this work, which demonstrates that rectangular channels provide the best overall performance while high aspect ratio and higher channel number lower thermal resistance but increase pressure drop. [27] Single-phase convective heat transfer and flow properties are strongly influenced by microchannel shape. Heat transfer and pressure drop are empirically correlated with aspect ratio and hydraulic diameter spacing for optimal laminar and turbulent performance. [28]

According to recent research, biomimetic cooling designs inspired by leaf veins greatly improve thermal-hydraulic performance. When tuned using nanofluids and surface alterations, composite bionic microchannels that combine vein-like fractal routes with honeycomb features demonstrate significant improvements in heat transmission, reaching up to a 64.5% increase in Nusselt number. Similar to this, leaf-vein and tree-root-inspired liquid-cooled plates use multi-objective optimization and structured flow distribution to reduce pressure drop, enhance uniformity, and lower peak temperatures. [29,30]

Nature-inspired flow topologies successfully reduce hydraulic penalties and nonuniform heating, according to recent biomimetic cooling experiments. Leaf-vein-based channel growth techniques dynamically adjust to hotspot locations, reducing overall pressure drop while achieving a peak temperature reduction of up to 40 K and significantly enhanced temperature uniformity. Similarly, in terms of temperature management and pressure loss, bionic leaf-vein liquid-cooled plates for battery systems routinely perform better than serpentine designs. Beyond vein networks, biomimetic surface patterns like microfeatures inspired by shark skin further improve heat transmission by modifying flow mixing and boundary-layer behavior, illustrating the wide potential of biomimicry for sophisticated thermal management. [31,32,33].

Bionic spider-web-inspired cold plates enhance thermal management in PEM fuel cells and lithium-ion batteries by improving temperature uniformity and reducing hotspots. CFD and numerical simulations show optimized channel widths and angles increase cooling efficiency, lower pressure drop, and mitigate thermal risks, demonstrating superior performance over traditional serpentine designs while maintaining operational stability. [34], [35] Biomimetic cooling systems draw inspiration from natural transport networks that achieve efficient flow distribution under strict energy and material constraints. By emulating optimal branching found in vascular and venation

systems, these designs enhance coolant delivery and heat dispersal, reducing hotspots and improving temperature uniformity in high-heat-flux devices. Studies show that leaf-vein, spider-cobweb, sharkskin, snowflake, and fractal-inspired structures significantly improve thermal-hydraulic performance, balancing heat transfer enhancement with pressure drop and manufacturability considerations. Bio-textured surface modification of straight-fin heat sinks is numerically and experimentally analyzed to enhance thermal performance without increasing size or weight. The textured fins demonstrate over 26% temperature reduction, ~34% lower thermal resistance, and a 21–40% increase in heat-sink effectiveness, particularly suitable for high-power electronic devices such as CPUs and GPUs.[36]

Thermal system performance is significantly improved by incorporating sophisticated diagnostic methods and structural changes. The necessity of exact geometric control in dynamic thermal management has been confirmed by infrared thermography investigation of plate heat exchangers, which has shown that flow arrangement directly controls transient temperature propagation and total heat transfer efficacy [37]. Another study employs two contrasting coolants to establish a comprehensive performance baseline. PG25, a conventional 25% propylene-glycol-water mixture with well-documented properties, provides a reliable reference for thermal-hydraulic behavior in compact systems. [38]

## 2. Methodology

We developed a three-dimensional, steady-state, conjugate heat transfer model to simulate the thermal-hydraulic performance of a liquid-cooled cold plate. Our approach consisted of four key phases: mathematical formulation, geometric definition, numerical solution, and verification.

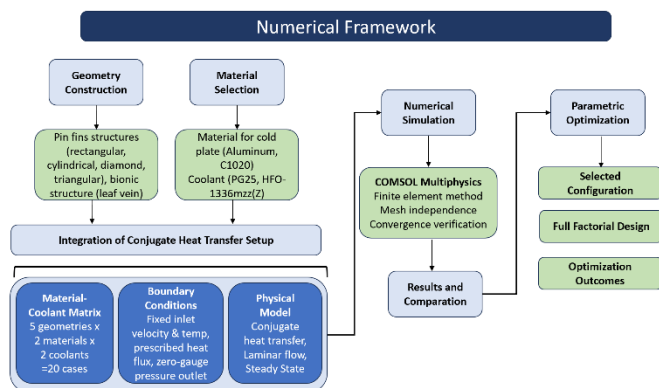


Fig- 1: Numerical framework

## 2.1. Mathematical Formulation

We modeled the fluid flow as incompressible and laminar using the continuity, Navier-Stokes, and energy equations. For the solid domains (base plate and fins), we solved the steady-state heat conduction equation. We enforced continuity of temperature and heat flux at all solid–fluid interfaces. We treated the working fluids as Newtonian with constant thermo-physical properties and neglected radiation, buoyancy, and phase change effects.

## 2.2. Geometric Configuration and Materials

We designed the cold plate with fixed outer dimensions: a base plate measuring 100 mm × 70 mm × 5 mm and an internal flow cavity of 80 mm × 65 mm × 3 mm. We investigated five internal fin architectures, each with a constant fin height of 3 mm: a bio-inspired leaf-vein design and four uniform pin-fin arrays (rectangular, diamond, cylindrical, and triangular cross-sections). For the pin-fin arrays, we maintained a constant pitch of 3 mm × 3 mm and fin density.

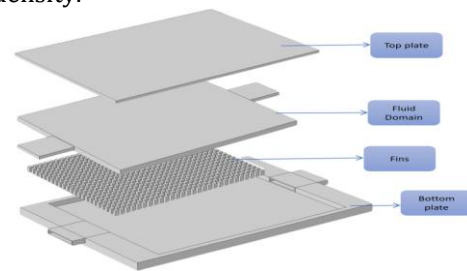


Fig- 2: Cutaway view of the cold plate geometry with internal cavity and fin region

We selected two solid materials, aluminum ( $k = 205 \text{ W/m}\cdot\text{K}$ ) and C1020 copper alloy ( $k = 390 \text{ W/m}\cdot\text{K}$ ), and two coolants, PG25 and HFO-1336mzz(Z), resulting in 20 simulation cases (5 geometries × 2 materials × 2 coolants)

Table-1: Thermo-physical properties of materials used in simulation

Materials	Density (kg/m <sup>3</sup> )	Heat Capacity Cp/(kg·K)	Thermal Conductivity W/(m·K)	Dynamic Viscosity (Pa·s)
Aluminum	2700	900	205	-
C1020	8960	385	390	-
PG25	1026	3700	0.472	0.00142
HFO-1336mzz(Z)	1361	1010	0.077	0.00038

As shown in Table 1, the selected materials and coolants provide a clear contrast in thermal conductivity and viscosity, enabling the isolation of their effects on conjugate heat transfer performance.

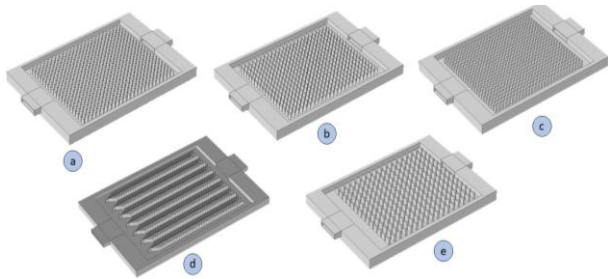


**Fig- 3:** Geometry structure of all the types of fins (a) cylindrical pin fins, (b) diamond-shaped pin fins, (c) rectangular-shaped pin fins, (d) leaf-vein fin structure, (e) triangular shaped pin fin structure

### 2.3. Numerical Solution and Boundary Conditions

We discretized the computational domain with an unstructured tetrahedral mesh and applied local refinement at solid–fluid interfaces and boundary layers. We performed the simulations using COMSOL Multiphysics software, employing a pressure-based segregated algorithm with the simple scheme for pressure–velocity coupling. We used second-order discretization for momentum and energy equations. We applied the following boundary conditions:

**Thermal:** We imposed a uniform heat flux of 171,428.6 W/m<sup>2</sup> (1200 W total) on the bottom surface of the base plate. We held the top surface at a constant temperature of 293.15 K and treated all other external surfaces as adiabatic.

**Flow:** We set a constant mass flow rate of 0.0347 kg/s at 293.15 K at the inlet and defined the outlet as a pressure-outlet (0 Pa gauge).

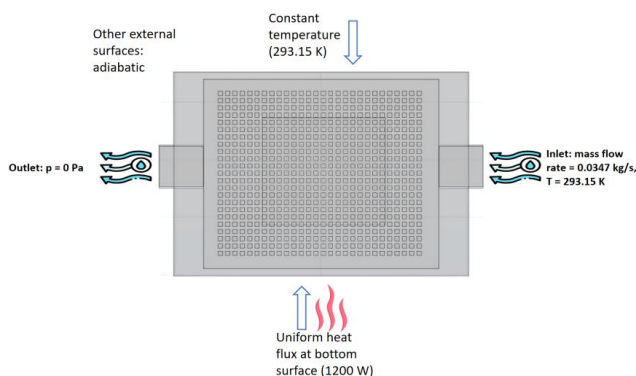


**Fig- 4:** Boundary conditions

We considered the solution converged when scaled residuals for all equations dropped below 10<sup>-6</sup> and key global monitors (maximum temperature and pressure drop) stabilized.

### 2.4. Verification and Validation

We conducted a grid independence study on two representative geometries: the rectangular pin-fin and leaf-vein designs. We tested three mesh densities and selected the medium mesh, which produced less than 1% variation in average base temperature and pressure drop. To validate the model physically, we compared the simulated temperature rise across the solid domain with a one-dimensional analytical conduction solution. The results showed consistent trends with deviations under 8 K, which we attribute to three-dimensional conduction and conjugate effects. We estimate the overall numerical uncertainty to be within ±3%

### 3. Results & Visualization

We present the thermal-hydraulic performance of five cold-plate fin architectures (leaf-vein, rectangular, diamond, cylindrical, and triangular pin-fins) using two solid materials (Al, C1020) and two coolants (PG25, HFO). Results were derived from 20 validated, steady-state conjugate heat transfer simulations.

**Table-2:** Summary of Thermal-Hydraulic Performance for All Configurations

Geometry	Material	Coolant	Thermal Resistance, R <sub>th</sub> (K/W)	Pressure Drop, ΔP (Pa)
Leaf-vein	C1020	PG25	0.01617	163.9
Leaf-vein	C1020	HFO-1336mzz(Z)	0.02026	66.5
Leaf-vein	Aluminum	PG25	0.02403	166.2
Leaf-vein	Aluminum	HFO-1336mzz(Z)	0.03052	64.6
Rectangular	C1020	PG25	0.01910	22.8
Rectangular	C1020	HFO-1336mzz(Z)	0.01499	47.4
Rectangular	Aluminum	PG25	0.01503	20.5
Rectangular	Aluminum	HFO-1336mzz(Z)	0.02110	33.4
Diamond	C1020	PG25	0.01217	8.2
Diamond	C1020	HFO-1336mzz(Z)	0.01605	48.9
Diamond	Aluminum	PG25	0.01750	10.0
Diamond	Aluminum	HFO-1336mzz(Z)	0.02086	104.8
Cylindrical	C1020	PG25	0.01310	38.8
Cylindrical	C1020	HFO-1336mzz(Z)	0.01625	51.2
Cylindrical	Aluminum	PG25	0.01994	13.9
Cylindrical	Aluminum	HFO-1336mzz(Z)	0.02278	102.3
Triangular	C1020	PG25	0.02953	6.8
Triangular	C1020	HFO-1336mzz(Z)	0.01995	44.2

Triangular	Aluminum	PG25	0.01854	14.4
Triangular	Aluminum	HFO-1336mzz(Z)	0.02802	43.6

This table consolidates the key performance metrics, enabling direct comparison of the trade-off between thermal resistance and hydraulic penalty across all tested geometry-material-coolant combinations.

### 3.1. Model Verification and Thermal Performance

Our model was verified via mesh independence, confirming less than 1% variation in key outputs. We validated the thermal solution by comparing the simulated temperature rise ( $\Delta T_{CFD}$ ) against a 1D analytical conduction estimate ( $\Delta T_{Analytical}$ ). CFD results were consistently higher (by 3–8 K) due to captured 3D and convective effects, confirming physical consistency. The lowest thermal resistance (0.01217 K/W) was achieved with the diamond pin-fin, C1020, and PG25, demonstrating superior heat spreading. In contrast, triangular and leaf-vein geometries showed higher thermal resistance due to flow maldistribution.

Hotspots correspond to areas of flow stagnation or reduced velocity, often found at channel bends or in the core heated zone. Diamond and rectangular geometries demonstrate superior thermal spreading, confining hotspots to smaller, cooler regions, while the leaf-vein design shows pronounced hotspots at its branching junctions due to uneven flow distribution. Coolant selection further modulates intensity, with PG25 providing smoother gradients than HFO, which exacerbates local heating in high-resistance geometries, directly linking flow physics to the observed thermal resistance trends.

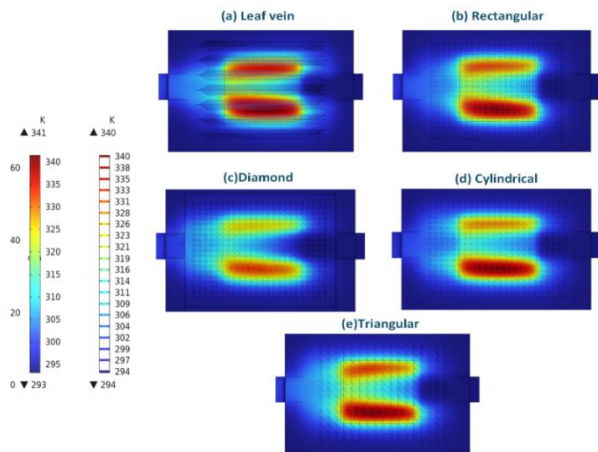


Fig- 5: Temperature contours of all geometries of Aluminum for PG25 coolant

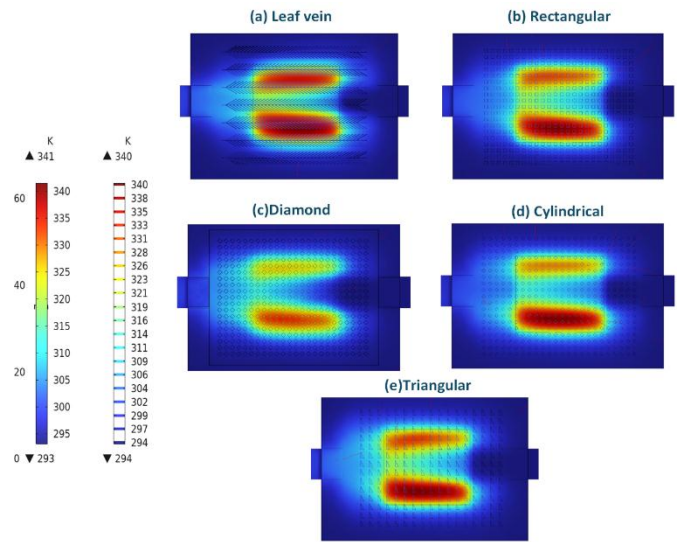


Fig- 7: Temperature contours of all geometries of Aluminum for HFO coolant

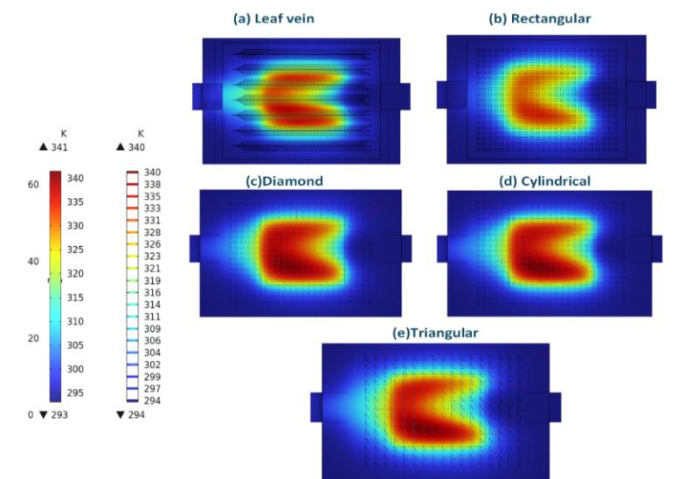


Fig- 8: Temperature contours of all geometries of C1020 for HFO coolant

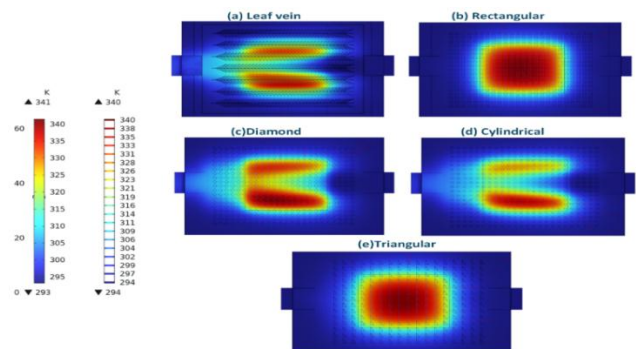


Fig- 6: Temperature contours of all geometries of C1020 for PG25 coolant

To provide a consolidated overview of the thermal-hydraulic performance, all results are summarized in a single performance matrix (Fig-8). This graph plots thermal resistance against pressure drop for all 20 simulation cases, clearly delineating the performance trade-off between all the geometries, materials, and both

the coolants. This visualization encapsulates the principal finding of this study that while geometry dictates the fundamental performance cluster, material and coolant selection act as critical modifiers within that design space.

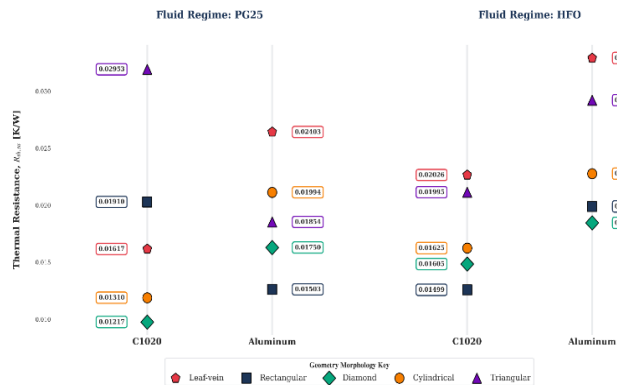


Fig- 9: Comparison of Thermal Resistance Performance of PG25 and HFO Coolants

### 3.2. Hydraulic Performance and Flow Analysis

Pressure drop was strongly geometry-dependent. The leaf-vein design imposed the highest penalty with PG25 ( $\Delta P \approx 164$  Pa), while diamond and triangular pin-fins were most hydraulically efficient ( $\Delta P < 10$  Pa). Coolant choice critically modulated this behavior: HFO reduced  $\Delta P$  in the complex leaf-vein channels by  $\sim 60\%$  but caused severe penalties ( $\Delta P > 100$  Pa) in diamond/cylindrical pin-fins with aluminum substrates due to conjugate thermal-viscous effects. Velocity field visualizations confirmed these trends, showing uniform flow in low- $\Delta P$  designs and significant separation/recirculation in high-resistance geometries.

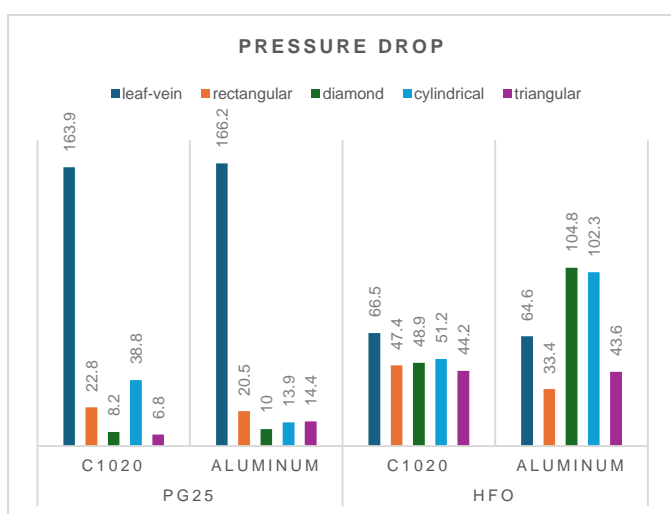


Fig- 10: Comparison of pressure drop values of PG25 and HFO

The velocity field visualizations directly link flow physics to hydraulic performance. Streamlines and contours reveal that low-pressure-drop geometries exhibit smooth, attached flow with minimal recirculation. In contrast, high-resistance cases display pronounced flow separation, jetting, and complex vortex formation. This mechanistic insight corroborates the quantitative pressure-drop data, confirming that adverse flow phenomena, driven by specific geometric and coolant interactions, are the primary cause of elevated pumping penalties.

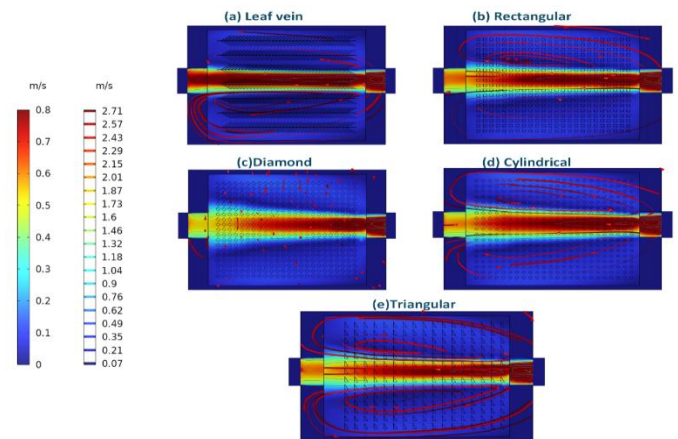


Fig- 11: Velocity field and streamline ribbons for all five geometries with PG25 coolant and C1020 substrate

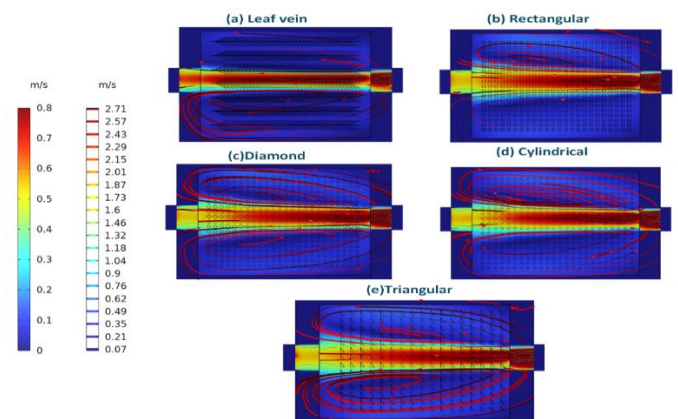


Fig- 12: Velocity field and streamline ribbons for all five geometries with PG25 coolant and aluminum substrate

Velocity fields for PG25 coolant visually explain the pressure drop trends. Diamond and triangular pin-fins exhibit smooth, attached flow ( $\Delta P < 10$  Pa), while the leaf-vein design shows complex recirculation and jetting ( $\Delta P \sim 164$  Pa). Substrate material has minimal hydraulic impact for PG25, though a slight thermal coupling effect is noted in the cylindrical fin case with aluminum.

For HFO coolant, velocity fields reveal distinct pressure-drop mechanisms. With C1020, the leaf-vein design shows smoother flow, explaining its lower  $\Delta P$  ( $\sim 67$  Pa). However, diamond and cylindrical pin-fins display severe flow

separation and high-velocity jets, corresponding to their elevated  $\Delta P$  (~49–51 Pa). The interaction is most severe with aluminum substrates. Diamond and cylindrical fins exhibit chaotic recirculation and intense jetting due to conjugate thermal effects, where the warmer wall lowers local HFO viscosity and increases shear, leading to very high  $\Delta P$  (>100 Pa). This visually confirms the critical role of material-fluid thermal coupling in hydraulic performance.

offering a competitive thermal resistance (0.01910 K/W) and moderate pressure drop (22.8 Pa). Designs with excellent single metrics (e.g., very low  $\Delta P$  or  $R_{th}$ ) were penalized in the combined ranking for poor performance in the other metric.

**Table-3:** p-Norm based multi-objective ranking of thermally and hydraulically reliable cold plate configurations

Configuration	Material	Coolant	Thermal Resistance ( $R_{th,sa}$ ) (K/W)	Pressure Drop ( $\Delta P$ ) (Pa)	p-Norm Distance ( $D_i$ )
Rectangular pin-fin	C1020	PG25	0.01910	22.8	0.326
Rectangular pin-fin	C1020	HFO-1336mzz(Z)	0.01499	47.4	0.414
Diamond pin-fin	C1020	HFO-1336mzz(Z)	0.01605	48.9	0.436
Cylindrical pin-fin	C1020	HFO-1336mzz(Z)	0.01625	51.2	0.461
Triangular pin-fin	C1020	PG25	0.02953	6.8	1.000
Diamond pin-fin	Aluminum	HFO-1336mzz(Z)	0.02086	104.8	1.078
Cylindrical pin-fin	Aluminum	HFO-1336mzz(Z)	0.02278	102.3	1.112

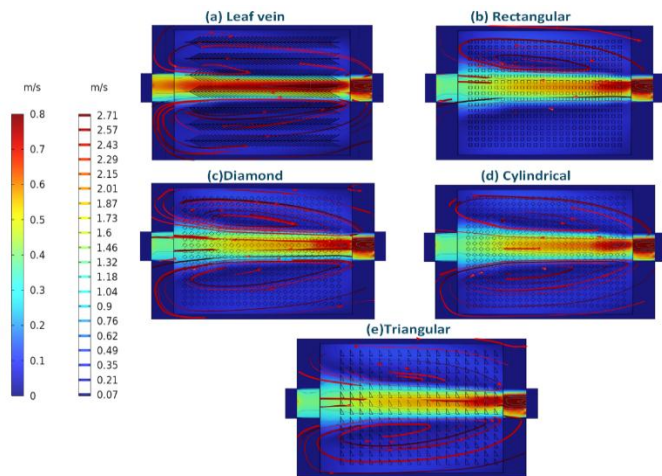


**Fig- 13:** Velocity field and streamline ribbons for all five geometries with HFO-1336mzz(Z) coolant and C1020 substrate

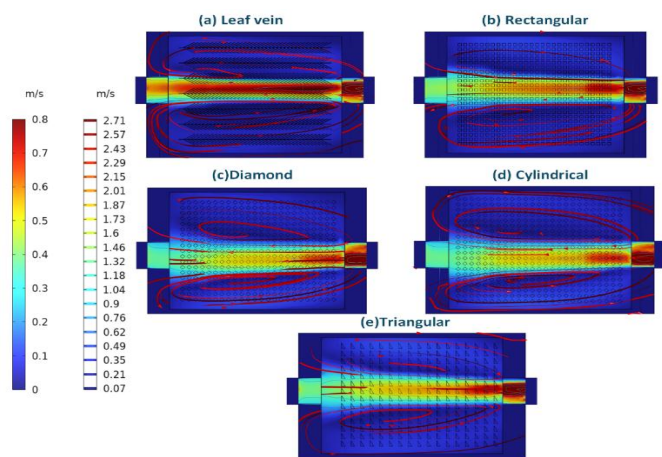


**Fig- 14:** Velocity field and streamline ribbons for all five geometries with HFO-1336mzz(Z) coolant and aluminum substrate

### 3.3. Multi-Objective Performance Ranking

We applied a p-Norm multi-objective analysis (balancing thermal resistance and pressure drop) to seven configurations that satisfied strict energy conservation. The rectangular pin-fin with C1020 and PG25 emerged as the most balanced design (p-Norm distance = 0.326),

### 3.4. Discussion of Key Trends

The results highlight that internal geometry is the primary driver of performance, with material and coolant acting as significant modifiers. Higher-conductivity materials (C1020) did not always yield lower thermal resistance, particularly with HFO, where conjugate effects altered near-wall flow. The optimal design depends on the weighting of thermal versus hydraulic objectives; however, the rectangular pin-fin with C1020/PG25 provides a robust, balanced solution for the imposed conditions.

### 4. PARAMETRIC OPTIMIZATION OF THE BASE DESIGN

Based on the multi-objective ranking, the rectangular pin-fin configuration with a C1020 substrate and PG25 coolant was selected as the baseline for parametric optimization. A full factorial design of experiments was conducted to isolate the effects of fin height ( $H_f$ ) and pin-fin pitch ( $S$ ) on thermal-hydraulic performance, with each parameter evaluated at three levels ( $H_f$ : 2.50, 2.75, 3.00 mm;  $S$ : 2.0, 2.5, 3.0 mm).

**Table-4:** Full factorial simulation matrix

Run	Fin Height ( $H_f$ )	Pitch ( $S_x = S_y$ )	Row Count (X×Y)
1	3 mm	3.0 mm	24×19
2	3 mm	2.5 mm	28×23
3	3 mm	2.0 mm	36×29
4	2.50 mm	3.0 mm	24×19
5	2.50 mm	2.5 mm	28×23
6	2.50 mm	2.0 mm	36×29
7	2.75 mm	3.0 mm	24×19
8	2.75 mm	2.5 mm	28×23
9	2.75 mm	2.0 mm	36×29

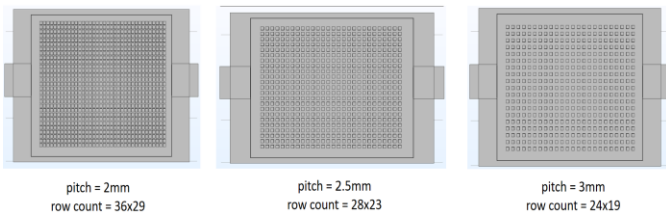


**Fig-15:** Top-view representation of rectangular pin-fin arrays illustrating the three pitch configurations used in the full factorial parametric study, with a constant effective finned footprint

#### 4.1. Optimization Results and Analysis

Fin height was the dominant parameter governing thermal performance. The configuration with  $H_f = 3.00$  mm and  $S = 2.0$  mm achieved the lowest thermal resistance (0.0123 K/W) and the best temperature uniformity. Pressure drop increased predictably with smaller pitch and greater height due to increased flow blockage, with values ranging from 4.9 Pa to 105.7 Pa across the design space.

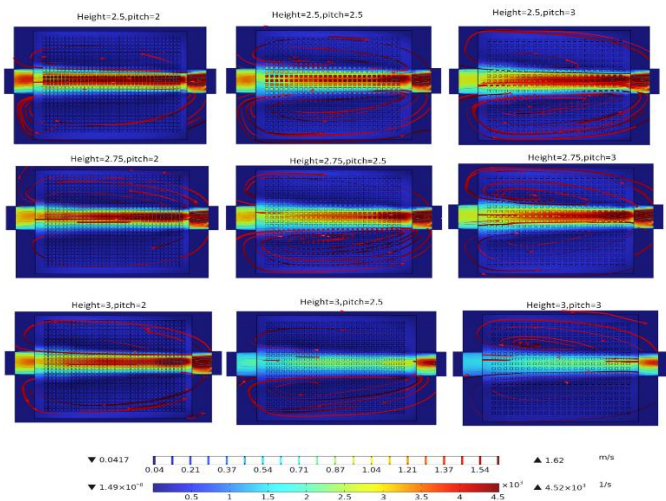


**Fig-16:** Velocity magnitude distribution for all nine rectangular pin-fin configurations showing the effect of fin height and pitch on flow behavior

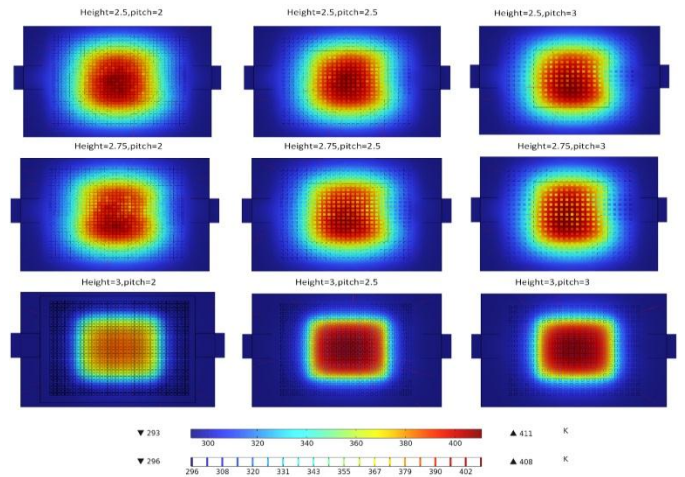
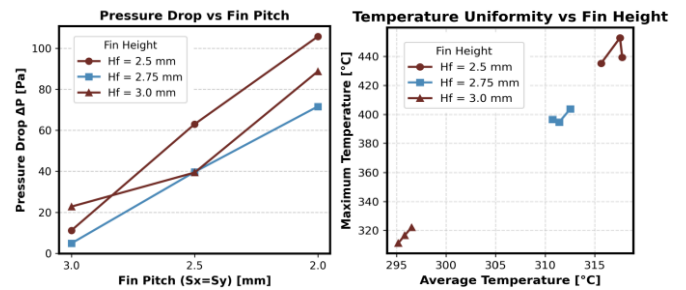


**Fig-17:** Temperature distribution for all nine rectangular pin-fin configurations illustrating the effect of fin height and pitch on thermal behavior

The results establish a clear trade-off: while reducing pitch enhances heat transfer, it imposes a significant hydraulic penalty. The optimal balance was confirmed to be the original baseline geometry ( $H_f = 3.00$  mm,  $S = 3.0$  mm), which provides excellent thermal performance ( $R_{th} = 0.01910$  K/W) with a manageable pressure drop (22.8 Pa), validating its selection from the initial comparative study.



The graphical representation of pressure drop reveals a clear trade-off, where decreasing pitch and increasing height consistently raise flow resistance. Corresponding temperature plots confirm that the highest fin density (2.0 mm pitch) coupled with maximum height (3.00 mm) achieves the lowest thermal resistance and most uniform temperature field, visually validating the quantitative performance trends.

#### 4.2. Summary of Optimized Design

The parametric study confirms that the rectangular pin-fin with C1020/PG25 is not only the most balanced design among fundamentally different architectures but is also robust near its original geometric parameters. No alternative combination of height and pitch within the studied range yielded a superior compromise, solidifying it as the recommended configuration for practical high heat-flux applications.

## 5. CONCLUSIONS

This numerical investigation systematically evaluated the thermal-hydraulic performance of five internal fin architectures under consistent operating constraints. The results demonstrate that geometry is the primary performance driver, with material and coolant selection acting as critical secondary modifiers. Through a validated conjugate heat transfer model and a subsequent p-Norm multi-objective analysis, the rectangular pin-fin configuration with a C1020 substrate and PG25 coolant was identified as the most balanced design, offering an optimal compromise between effective heat removal ( $R_{th} = 0.01910$  K/W) and acceptable flow resistance ( $\Delta P = 22.8$  Pa). These findings provide a foundational guideline for the design of efficient, practical liquid-cooled cold plates for high heat-flux thermal management applications.

## REFERENCES

- [1] B. R. R. Bapu, S. Kayalvizhi, and S. Murugavalli, "Two phase cooling with nano-fluid for highly dense electronic systems-on-chip – A pilot study," *Microelectron. Reliab.*, vol. 108, p. 113640, May 2020, doi: 10.1016/j.microrel.2020.113640.
- [2] S. Zhu, Z. Zhang, H. Chen, and Y. Li, "Numerical Investigation of a Bionic Vapor Chamber Based on Leaf Veins for Cooling Electronic Devices," *Sustainability*, vol. 15, no. 2, 2023, doi: 10.3390/su15021125.
- [3] J. Xu, K. Zhang, J. Duan, J. Lei, and J. Wu, "Systematic Comparison on Convective Heat Transfer Characteristics of Several Pin Fins for Turbine Cooling," *Crystals*, vol. 11, no. 8, 2021, doi: 10.3390/cryst11080977.
- [4] M. H. Ruhaidi and N. Darlis, "Analysis of Pin Fin Shapes on Thermal Performances in Microchannel Heat Sink using Computational Fluid Dynamics (CFD)," *Prog. Eng. Appl. Technol.*, vol. 6, no. 1, pp. 742–751, Apr. 2025.
- [5] B. M. Diaconu, M. Cruceru, and L. Anghelescu, "Phase Change Materials—Applications and Systems Designs: A Literature Review," *Designs*, vol. 6, no. 6, 2022, doi: 10.3390/designs6060117.
- [6] B. Zalba, J. M. Marín, L. F. Cabeza, and H. Mehling, "Review on thermal energy storage with phase change: materials, heat transfer analysis and applications," *Appl. Therm. Eng.*, vol. 23, no. 3, pp. 251–283, 2003, doi: [https://doi.org/10.1016/S1359-4311\(02\)00192-8](https://doi.org/10.1016/S1359-4311(02)00192-8).
- [7] Y. Li, X. Yang, X. Tian, and T. Yu, "Capillary-Driven Boiling Heat Transfer on Superwetting Microgrooves," *ACS Omega*, Sep. 2022, doi: 10.1021/acsomega.2c05381.
- [8] M. Yao, M. Zebarjadi, and C. P. Opeil, "Experimental determination of phonon thermal conductivity and Lorenz ratio of single crystal metals: Al, Cu, and Zn," *J. Appl. Phys.*, vol. 122, no. 13, p. 135111, Oct. 2017, doi: 10.1063/1.4997034.
- [9] A. Zhang and Y. Li, "Thermal Conductivity of Aluminum Alloys—A Review," *Materials*, vol. 16, p. 2972, Apr. 2023, doi: 10.3390/ma16082972.
- [10] J. Valois, G. Nellis, and J. Pfothner, "Characterization of the thermal properties of OFHC copper at cryogenic temperature," *IOP Conf. Ser. Mater. Sci. Eng.*, vol. 1301, p. 012167, May 2024, doi: 10.1088/1757-899X/1301/1/012167.
- [11] A. R. Dhumal, A. P. Kulkarni, and N. H. Ambhore, "A comprehensive review on thermal management of electronic devices," *J. Eng. Appl. Sci.*, vol. 70, no. 1, p. 140, Nov. 2023, doi: 10.1186/s44147-023-00309-2.
- [12] J. Pandit, M. Thompson, S. Ekkad, and S. Huxtable, "Effect of pin fin to channel height ratio and pin fin geometry on heat transfer performance for flow in rectangular channels," *Int. J. Heat Mass Transf.*, vol. 77, pp. 359–368, Oct. 2014, doi: 10.1016/j.ijheatmasstransfer.2014.05.030.
- [13] F. Alnaimat and M. Ziauddin, "Experimental investigation of heat transfer in pin-fins heat sinks for cooling applications," *Heat Mass Transf.*, vol. 57, Aug. 2020, doi: 10.1007/s00231-020-02947-1.
- [14] M. Alteneiji, A. Raafat, and S. K. Alnuaimi, "Impact of height and secondary flow patterns of circle, square and triangle shaped pin fins on microchannel heat sinks performance," *Therm. Sci. Eng. Prog.*, vol. 67, p. 104166, 2025, doi: <https://doi.org/10.1016/j.tsep.2025.104166>.
- [15] K. Madi, A. Raafat, and S. A. Nuaimi, "Enhanced thermal management in microelectronic cooling: A study on pairing multiple pin-fin shapes in microchannel heat sinks," *Int. J. Thermofluids*, vol. 28, p. 101283, 2025, doi: <https://doi.org/10.1016/j.ijft.2025.101283>.
- [16] Arjun Kozhikkatil Sunil and Kumar Rakesh, "Optimization of micro pin-fin heat sink with staggered arrangement," vol. 22, no. 6, pp. 2919–2931, 2018.
- [17] R. Niranjana, O. Singh, and J. Ramkumar, "Thermo-Hydraulic Performance of Square Micro Pin Fins under Forced Convection," *Int. J. Heat Technol.*, vol. 39, pp. 170–178, Feb. 2021, doi: 10.18280/ijht.390118.
- [18] Numerical investigation of pin-fin thermal performance for staggered and inline arrays at low Reynolds number.
- [19] N. H. Naqiuddin, L. H. Saw, M. C. Yew, F. Yusof, T. C. Ng, and M. K. Yew, "Overview of micro-channel design for high heat flux application," *Renew. Sustain. Energy Rev.*,

- vol. 82, pp. 901-914, 2018, doi: <https://doi.org/10.1016/j.rser.2017.09.110>.
- [20] M. Hekmatara and M. Kharati-Koopae, "Numerical study of the influence of pin fin arrangement and volume fraction on the heat transfer and fluid flow phenomena within open microchannels," *Int. Commun. Heat Mass Transf.*, vol. 155, p. 107595, 2024, doi: <https://doi.org/10.1016/j.icheatmasstransfer.2024.107595>.
- [21] A. Abdoli, G. Jimenez, and G. S. Dulikravich, "Thermo-fluid analysis of micro pin-fin array cooling configurations for high heat fluxes with a hot spot," *Int. J. Therm. Sci.*, vol. 90, pp. 290-297, 2015, doi: <https://doi.org/10.1016/j.ijthermalsci.2014.12.021>.
- [22] H. M. Jaffal, H. S. Jebur, and A. A. Hussein, "Numerical and Experimental Investigations on the Performance Characteristics for Different Shapes Pin Fin Heat Sink," 2018. [Online]. Available: <https://api.semanticscholar.org/CorpusID:211018765>
- [23] Y. Alihosseini, M. Z. Targhi, M. M. Heyhat, and N. Ghorbani, "Effect of a micro heat sink geometric design on thermo-hydraulic performance: A review," *Appl. Therm. Eng.*, vol. 170, p. 114974, 2020, doi: <https://doi.org/10.1016/j.applthermaleng.2020.114974>.
- [24] H. Sallar, M. Irfan, M. M. Khan, and M. W. Shahzad, "Hydro-thermal performance of an I-shaped pin fin microchannel heat sink with variable pin fin height, thickness and orientation," *Int. Commun. Heat Mass Transf.*, vol. 160, p. 108256, 2025, doi: <https://doi.org/10.1016/j.icheatmasstransfer.2024.108256>.
- [25] W. Qu and I. Mudawar, "Experimental and numerical study of pressure drop and heat transfer in a single-phase micro-channel heat sink," *Int. J. Heat Mass Transf.*, vol. 45, no. 12, pp. 2549-2565, 2002, doi: [https://doi.org/10.1016/S0017-9310\(01\)00337-4](https://doi.org/10.1016/S0017-9310(01)00337-4).
- [26] A. G. Fedorov and R. Viskanta, "Three-dimensional conjugate heat transfer in the microchannel heat sink for electronic packaging," *Int. J. Heat Mass Transf.*, vol. 43, no. 3, pp. 399-415, 2000, doi: [https://doi.org/10.1016/S0017-9310\(99\)00151-9](https://doi.org/10.1016/S0017-9310(99)00151-9).
- [27] H. Wang, Z. Chen, and J. Gao, "Influence of geometric parameters on flow and heat transfer performance of micro-channel heat sinks," *Appl. Therm. Eng.*, vol. 107, pp. 870-879, 2016, doi: <https://doi.org/10.1016/j.applthermaleng.2016.07.039>.
- [28] X. F. Peng and G. P. Peterson, "Convective heat transfer and flow friction for water flow in microchannel structures," *Int. J. Heat Mass Transf.*, vol. 39, no. 12, pp. 2599-2608, 1996, doi: [https://doi.org/10.1016/0017-9310\(95\)00327-4](https://doi.org/10.1016/0017-9310(95)00327-4).
- [29] L. Yue, C. Qi, and M. Tang, "A novel composite bionic leaf vein and honeycomb microchannel heat sink applied for thermal management of electronic components," *Appl. Therm. Eng.*, vol. 252, p. 123716, 2024, doi: <https://doi.org/10.1016/j.applthermaleng.2024.123716>.
- [30] H. Xia, J. Wang, Y. Shen, and K. Fang, "A liquid-cooled plate based on bionic flow channels evolved from the shape of leaf veins and tree roots," *Int. J. Therm. Sci.*, vol. 208, p. 109468, 2025, doi: <https://doi.org/10.1016/j.ijthermalsci.2024.109468>.
- [31] X. Wang, Z. Zhou, H. Li, G. Xie, L. Meng, and Z. Zhang, "Programmed constructions of novel bionic heat sinks inspired by leaf venation pattern," *Int. J. Heat Mass Transf.*, vol. 251, p. 127353, 2025, doi: <https://doi.org/10.1016/j.ijheatmasstransfer.2025.127353>.
- [32] Sun Guangqiang, Li Zhiqiang, Wang Fang, Liu Xianfei, and Ba Yichun, "Study on cooling of bionic leaf-vein channel liquid-cooled plate for lithium-ion battery pack," vol. 28, no. 5, pp. 3907-3919, 2024.
- [33] K. Wang, Y. Shi, J. Chen, and Y. Dai, "A Biomimetic Microchannel Heat Sink for Enhanced Thermal Performance in Chip Cooling," *Biomimetics*, vol. 10, no. 7, 2025, doi: 10.3390/biomimetics10070459.
- [34] J. Wang, X. Liu, F. Liu, Y. Liu, F. Wang, and N. Yang, "Numerical optimization of the cooling effect of the bionic spider-web channel cold plate on a pouch lithium-ion battery," *Case Stud. Therm. Eng.*, vol. 26, p. 101124, 2021, doi: <https://doi.org/10.1016/j.csite.2021.101124>.
- [35] X. Yang et al., "Model-based and data-driven approaches for PEMFC bionic spider web channel cold plate structure design and liquid cooling performance optimization study," *Renew. Energy*, vol. 256, p. 123957, 2026, doi: <https://doi.org/10.1016/j.renene.2025.123957>.
- [36] E. Foronda, F. J. Ramírez-Gil, Á. Delgado-Mejía, L. M. Ballesteros, J. S. Rudas, and L. C. Olmos-Villalba, "Thermal enhancement of heat sinks with bio-inspired textured surfaces," *Therm. Sci. Eng. Prog.*, vol. 46, p. 102170, 2023, doi: <https://doi.org/10.1016/j.tsep.2023.102170>.
- [37] M. Bobič, B. Gjerek, I. Golobič, and I. Bajsić, "Dynamic behaviour of a plate heat exchanger: Influence of temperature disturbances and flow configurations," *Int. J. Heat Mass Transf.*, vol. 163, p. 120439, 2020, doi: <https://doi.org/10.1016/j.ijheatmasstransfer.2020.120439>.

[38] A. Alenezi, H. M. Ali, and P. E. Phelan, "Experimental investigation of the effect of ultrasonic waves on heat transfer enhancement and pressure drop for propylene glycol/water mixtures in a rectangular minichannel heat sink," *Appl. Therm. Eng.*, vol. 267, p. 125717, 2025, doi: <https://doi.org/10.1016/j.applthermaleng.2025.125717>.